Verification of a two-phase flow code based on an homogeneous model

Philippe Helluy, Olivier Hurisse, Erwan Le Coupanec

Verification of a two-phase flow code based on an homogeneous model.

Philippe Helluy°, Olivier Hurisse†, Erwan Le Coupanec†

°*IRMA, Université de Strasbourg, 7 rue René-Descartes, 67000 Strasbourg, France.*

†*EDF R&D MFEE, 6 quai Watier, 78400 Chatou, France.*

helluy@math.unistra.fr, olivier.hurisse@edf.fr, erwan.lecoupanec@edf.fr

Abstract

We present some verification test cases applied to a code developed at EDF R&D for the simulation of two-phase flows with mass transfer. The aim of this code is to allow the simulation of a wide range of industrial situations by considering all the thermodynamic disequilibria between the phases - pressure, temperature and chemical potential- and by assuming the kinematic equilibrium - a single velocity for both phases. The underlying homogeneous model [1, 13] is based on the Euler system of equations supplemented by a complex pressure law describing the behaviour of the mixture of the two phases. Different first-order schemes are compared on the basis of two analytical solutions: a classical Riemann problem and a steady-state heated pipe test.

Key words : Homogeneous model, two-phase flows, verification.

1 Introduction

The production of electric power through pressurized water nuclear reactor, as many other industrial processes, is associated with the control of the mass transfer phenomena between liquid water and its vapor. The numerical simulation of two-phase flows including phase change is then an important challenge though it is a difficult task. For this purpose, several kinds of models have been proposed for approximately 50 years. The model retained in the sequel has been proposed quite recently [1]. This two-phase flow model accounts for the complete thermodynamical disequilibrium - namely the pressure, temperature and chemical potential disequilibrium - but makes the assumption that both phases have the same velocity. It is based on the Euler system of equations supplemented by a complex pressure law describing the behaviour of the mixture of the two phases. This pressure law depends on

three mixture fractions which define the thermodynamical disequilibrium between the phases, and the return to equilibrium is achieved by three source terms. In the sequel, the verification test cases do not account for these source terms and the focus is put on the convective terms of the model.

In [13], the behaviour of some explicit first-order schemes has been compared on two Riemann problems, which are unsteady test cases. The aim of the present paper is to extend this verification process to a steady-state analytical test-case and to investigate the behaviour of a first-order semi-implicit scheme, based on a fractional step algorithm [19]. The latter class of schemes is known to handle more accurately steady-state situations than the first-order explicit schemes. Besides this semi-implicit scheme, the VFRoe-ncv scheme and the Rusanov scheme already used in [2] are retained here. In order to improve the accuracy of the VFRoe-ncv scheme on the contact waves, a centered-pressure correction is proposed on the basis of the work [4].

Two analytical test cases have been retained here. Both are representative of industrial applications at high pressure and temperature. First, as in [13] the different schemes have been used to compute approximate solutions of a Riemann problem. This unsteady test case allows to test the scheme for breach simulations which are part of the validation test cases for industrial codes in the nuclear domain. The second test case is a rough representation of the way a core or a steam generator operates. It consists in computing the steady state reached by a mixture of liquid and water which is heated by an external source. The solution proposed in [14] for compressible single-phase flow is thus extended to two-phase flows without return to equilibrium.

2 The homogeneous model

In the sequel the two-phase-flow homogeneous model [1, 15, 13] is based on the Euler set of equations. The thermodynamic behaviour of the mixture is ruled by two ingredients: three mixture fractions $Y = (\alpha, y, z)^\top$, which are respectively the volume fraction, the mass fraction and the energy fraction; and a mixture pressure law $P = \mathcal{P}(Y, \tau, e)$ defined through the Gibbs relation on the entropy of the mixture. The thermodynamic disequilibrium and the return to equilibrium are taken into account by source terms Γ_Y on the fraction equations. The whole model then reads:

$$\left\{\begin{array}{l} \dfrac{\partial}{\partial t}(\rho Y) + \dfrac{\partial}{\partial x}(\rho U Y) = \rho \Gamma_Y \\ \dfrac{\partial}{\partial t}(\rho) + \dfrac{\partial}{\partial x}(\rho U) = 0 \\ \dfrac{\partial}{\partial t}(\rho U) + \dfrac{\partial}{\partial x}\left(\rho U^2 + P\right) = 0 \\ \dfrac{\partial}{\partial t}(\rho E) + \dfrac{\partial}{\partial x}(\rho U E + U P) = 0. \end{array}\right. \tag{1}$$

The velocity of the mixture is denoted by U. No kinematic disequilibrium is taken into account, then U also represents the velocity of each phase. We note: $\rho = 1/\tau$ the density of the mixture, where τ is the specific volume, $E = e + U^2/2$ the specific total energy of the mixture and e the specific internal energy of the mixture. The pressure law $\mathcal{P}$ is:

$$\mathcal{P}(Y, \tau, e) = \frac{\frac{\alpha}{T_l} P_l + \frac{(1-\alpha)}{T_v} P_v}{\frac{z}{T_l} + \frac{1-z}{T_v}}, \tag{2}$$

where the phasic pressures $P_k = \mathcal{P}_k(\tau_k, e_k)$ and temperatures $T_k = \mathcal{T}_k(\tau_k, e_k)$ must be given by the user, with $e_l = ze/y$, $e_v = (1-z)e/(1-y)$, $\tau_l = \alpha\tau/y$, $\tau_v = (1-\alpha)\tau/(1-y)$ if Y represents the fraction of phase l. The source terms Γ_Y are defined in agreement with the second principle of thermodynamics [1, 15, 13], but they are not considered here for the proposed verification test cases and we set here: $\Gamma_Y = 0$. In the sequel, a Stiffened Gas equation of states will be used for each phase:

$$\mathcal{P}_k(\tau_k, e_k) = \frac{e_k}{\tau_k}(\gamma_k - 1) - \Pi_k \gamma_k \qquad \text{and} \qquad \mathcal{T}_k(\tau_k, e_k) = \frac{e_k - \Pi_k \tau_k}{C_{v,k}},$$

where γ_k, Π_k and $C_{v,k}$ are parameters. For these Stiffened Gas equations of states, the model (1) is hyperbolic if the phasic temperatures are non-negative. Values of the thermodynamical coefficients will be given in section 4. More details on the whole model can be found in [1, 13].

3 Numerical schemes

The overall numerical scheme follows a fractional step algorithm in which convective terms and source terms are treated successively [13]. Since source terms have been omitted in the sequel, we only describe below the numerical schemes that have been implemented to account for the convective part of the model (1). The numerical approximations are obtained by using two different types of first-order finite-volume schemes [5]:

- approximate godunov schemes which are explicit,
- and a semi-implicit fractional step scheme.

Considering the first class of schemes, three different schemes have been investigated. As proposed in [13] a VFRoe-ncv scheme [2] is used to compute the numerical fluxes at the interface between two cells. The linearised problem at the interface is solved by considering the variables (Y, τ, U, P). This algorithm is supplemented with the entropic correction proposed in [12]. Moreover, a partial WFRoe scheme [9] is performed to improve the prediction of the speed of the contact wave in the linearised problem at the interface between two cells. Otherwise, non-symmetric behaviours have been observed on some test cases, in particular for bubble collapse. This scheme will be nicknamed here VFROENCV. In order to improve the accuracy of this scheme, another version has been implemented on the basis of the idea of [4]. The interfacial pressure issued from the linearised Riemann problem is mixed with a centered pressure chosen as the mean of the pressure of the left (L) and right

(R) cells. The blending function $f_b(M)$ for the pressure is based on the local Mach number $M = |u_{LR}|/max(C_L, C_R)$, where u_{LR} is the interfacial WFRoe-ncv velocity. C_L and C_R are respectively the left and right sound speeds. We have chosen the function:

$$f_b(M) = \begin{cases} \frac{1-cos(\Pi M/M_{lim})}{2}, & \text{if} \quad M \leq M_{lim}, \\ 1, \quad \text{otherwise.} \end{cases} \tag{3}$$

The modified interfacial pressure P^*_{LR} used to compute the numerical fluxes is then:

$$P^*_{LR} = f_b(M)P_{LR} + (1 - f_b(M))\frac{P_L + P_R}{2};$$

where P_{LR} is the interfacial pressure computed by the VFROENCV scheme, P_L and P_R the left and right pressures. The parameter M_{lim} is the limit mach number above which the pressure correction is not activated. The influence of this parameter on the results will not be discussed here even if it is an important parameter. The results of section 4 have been obtained with $M_{lim} = 0.25$. This scheme will be nicknamed here VFROENCV-C. More details about VFROENCV and VFROENCV-C schemes can be found in appendix B. The Rusanov scheme [17] is also considered as it remains a reference scheme, it will be denoted by RUSANOV.

The VFRoe-ncv scheme is an explicit scheme. In order to maintain the stability of the numerical approximations a CFL condition must be fulfilled by the time-step. Moreover, it is known that for low mach-number situations discrepancies may be observed. These limitations can be strong drawbacks for industrial applications.

The semi-implicit scheme [7] relies on a fractional step method [19] which consists in 4 main steps: a density step, a momentum step, a total energy step and a mixture fraction convection step. The density step consists in solving the continuity equation turned into a pressure equation (thanks to a linearization of the density). This step yields a predicted pressure and allows to update the mass flux and the density. The momentum step then consists in solving the momentum balance equation considering the explicit gradient of the predicted pressure and the updated mass flux. The total energy step finally consists in solving the total energy balance equation considering the updated mass flux. The internal energy can at last be deduced and is taken into account together with the updated density (from the density step) in order to update the pressure. This scheme is detailed in appendix C. It will be nicknamed here SEMI-IMP.

4 Numerical results

The behavior of the schemes is compared on two different test cases: an unsteady test case and a steady-state test case. For both tests we use the same parameters

for the phasic equation of states:

$$\begin{array}{cc} Cv,v = 4.477815802223535\ 10^3\ J/kg/K & Cv,l = 1.395286166711847\ 10^3\ J/kg/K \\ \gamma_v = 1.084875362318841 & \gamma_l = 1.665128030303030 \\ \Pi_v = 0.0 & \Pi_l = 3.725876146842836\ 10^8\ Pa \end{array} \tag{4}$$

These parameters have been computed to be representative of steam-water flows around 81 $bars$ and at saturation ($T_{sat}(81\ bars) = 569\ K$).

The approximations obtained by the schemes on uniform meshes have been compared with the analytical solution in terms of the L_1 error:

$$err(\phi, T) = \frac{\sum_{i=1}^{N} |\phi^{approx}(T, x_i) - \phi^{exact}(T, x_i)|}{\sum_{i=1}^{N} |\phi^{exact}(T, x_i)|}, \tag{5}$$

for the variables $\phi = \{\alpha, y, z, \rho, U, P\}$. This error is computed at the final time t for the unsteady test case and when convergence in time is assumed to be reached for the steady case (see section 4.2 for details on the convergence criterium).

4.1 A Riemann problem test case

As in [13], we consider here a Riemann problem consisting in a U-contact wave and a $U + C$-shock wave. The $U - C$-wave is a ghost wave. The domain is $[0, 1\ m]$ and the initial discontinuity is located at $x_d = 1/2\ m$. The boundary conditions are Dirichlet conditions filled with the exact solution. The exact solution is composed of the left and right uniform states, separated by an uniform intermediate state. The intermediate state in table 1 represents the analytical solution between the U-contact and the $U+C$-shock wave, that is for: $(x-x_d)/t > 5\ m/s$ and $(x-x_d)/t < \sigma$, where the shock speed is:

$$\sigma = 857.774166173626327\ m/s.$$

The left state represents the solution for $(x - x_d)/t < 5\ m/s$ and the right state for $(x - x_d)/t > \sigma$. The solution is plotted on figure (2) at time $t = 2.\ 10^{-4}\ s$. The error between the numerical approximations and the exact solution is computed at this time. The approximate solutions have been computed with the four different

	Left state	Intermediate state	Right state
α	$1.38006860749359000\ 10^{-1}$	$1.48006860749359009\ 10^{-1}$	$1.48006860749359009\ 10^{-1}$
y	$7.84348344805274079\ 10^{-3}$	$8.84348344805273995\ 10^{-3}$	$8.84348344805273995\ 10^{-3}$
z	$1.51281566759211995\ 10^{-2}$	$1.61281566759211986\ 10^{-2}$	$1.61281566759211986\ 10^{-2}$
$\rho\ (kg/m^3)$	728	738	733
$U\ (m/s)$	5.0	5.0	-0.817013411825560532
$P\ (Pa)$	$7.69\ 10^6$	$7.69\ 10^6$	$4.02907811372492649\ 10^6$

Figure 1: States for the first Riemann problem.

schemes: RUSANOV, VFROENCV, VFROENCV-C and SEMI-IMP. The meshes have from 50 to 200000 regular cells, except for the SEMI-IMP scheme (up to 50000

cells). The error defined in (5) is plotted on figures 3 and 4 and the different approximate solutions are compared on figure 5 for a mesh with 800 cells and a time step chosen such that $CFL_{U+C} = 0.5$.

Considering figure (3), it can be noted that all the schemes have almost the same accuracy on coarse meshes, except the RUSANOV scheme that is less accurate for α and τ. Nonetheless, when the mesh is refined, the VFROENCV-C scheme widens the gap with the other schemes for the variable P, U and τ. Up to 200000 cells the asymptotic order of convergence 1/2 is not yet reached with VFROENCV-C for P and U. On the last three meshes the convergence rate is close to 1 for P and U, which indicates that the scheme is very accurate on the contact wave. The SEMI-IMP scheme with a time step chosen such that $CFL_{U+C} = 0.5$ is close to the VFROENCV scheme. Moreover, figure (4) shows that increasing the time-step for SEMI-IMP leads to a loss of accuracy.

Besides the error analysis, one can observe on figure (5) that the schemes have very different behaviours when a discontinuity is approximated, see figure (6).

- **The $U - C$ ghost wave** (on the left on figure (6)).
  From an analytical point of view all the variables remain constant when passing through the wave $U - C$, but for all the tested schemes a "numerical wave" $U - C$ can be observed. These discrepancies disappear when the mesh is refined, but they can be noticeable on coarse meshes. The VFROENCV-C scheme shows very strong oscillations with respect to the other schemes, and the SEMI-IMP scheme at $CFL_{U+C} = 0.5$ is very close to the VFROENCV scheme which remains quite accurate.

- **The contact wave** (in the middle on figure (6)).
  Through the contact wave, pressure and velocity are constant in the analytical solution. The VFROENCV scheme presents small discrepancies on this wave. The accuracy is then very good despite the fact that the pressure law does not fulfil the requirement to ensure the preservation of P and U as exposed in [8]. The VFROENCV-C scheme generates oscillations on both sides of the contact wave, whereas the SEMI-IMP scheme presents a pressure over-shoot combined with small oscillations.

- **The shock wave** (on the right on figure (6)).
  Both SEMI-IMP and VFROENCV-C approximations have oscillations at the shock location, but their order of magnitude is 100 times less for the former than for the latter. They are thus almost negligible for the SEMI-IMP scheme in comparison with the pressure jump through the schock wave ($\sim 36\ 10^5\ Pa$).

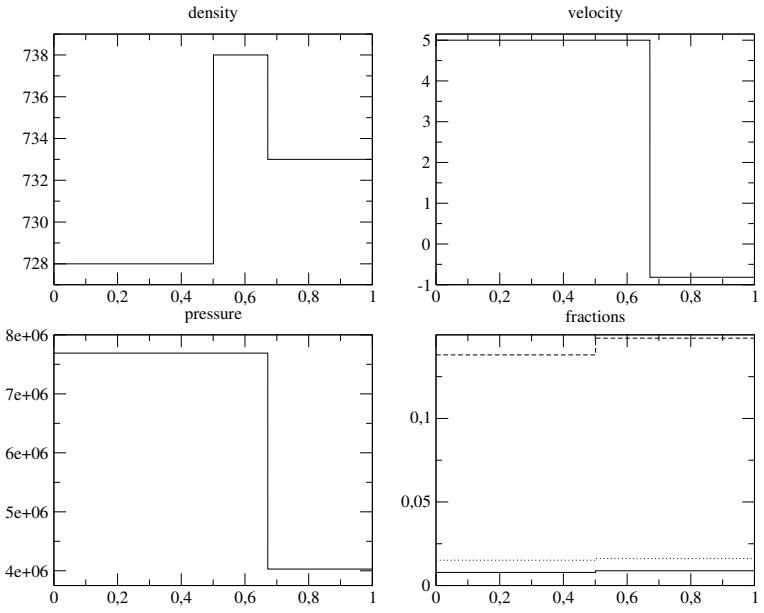

Figure 2: Analytical solution at time $t = 2.\ 10^{-4}\ s$ for the Riemann problem of section 4.1.

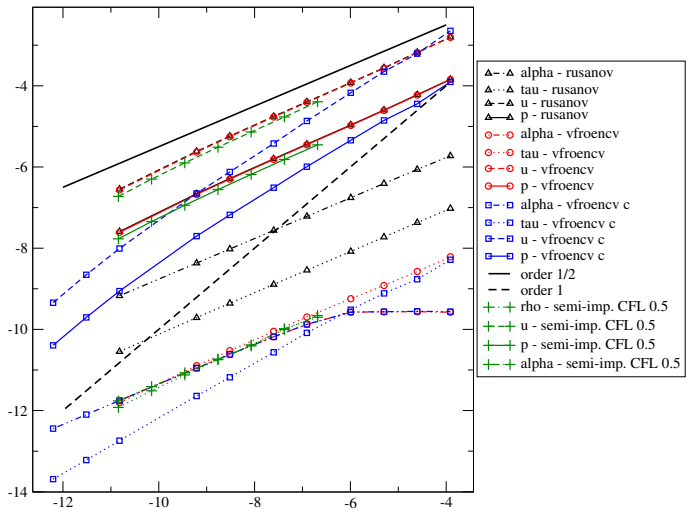

Figure 3: Convergence curves for all the schemes for the Riemann problem: ln() of the L^1 error norm (5) with respect to $\ln(1/N)$ (N number of cells). The CFL_{U+C} is equal to 0.5 for all the schemes.

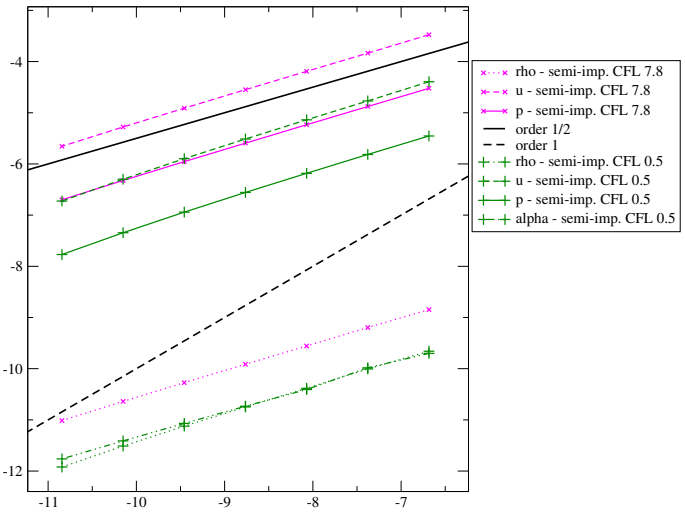

Figure 4: Convergence curves for the SEMI-IMP scheme for the Riemann problem: ln() of the L^1 error norm (5) with respect to $\ln(1/N)$ (N number of cells). The results obtained with $CFL_{U+C} = 0.5$ (green) and $CFL_{U+C} = 7.8$ (magenta) are plotted.

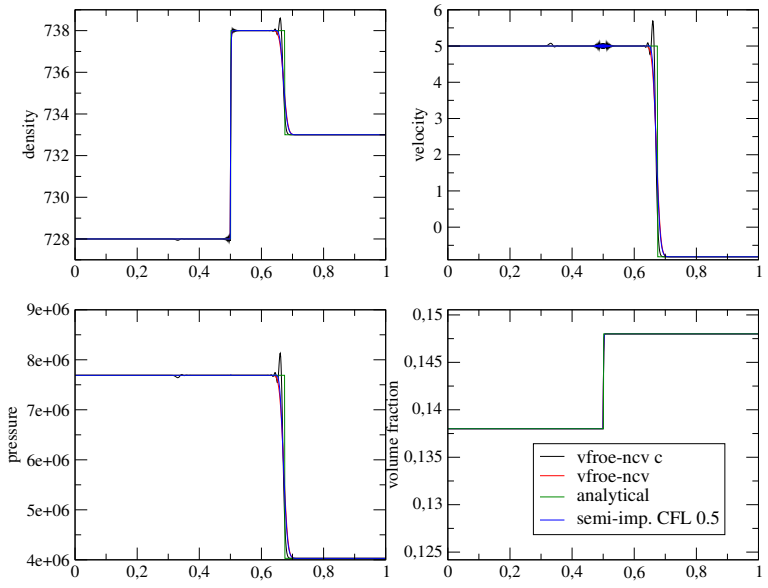

Figure 5: Comparison of the approximate solutions on a mesh with 800 cells and $CFL_{U+C} = 0.5$.

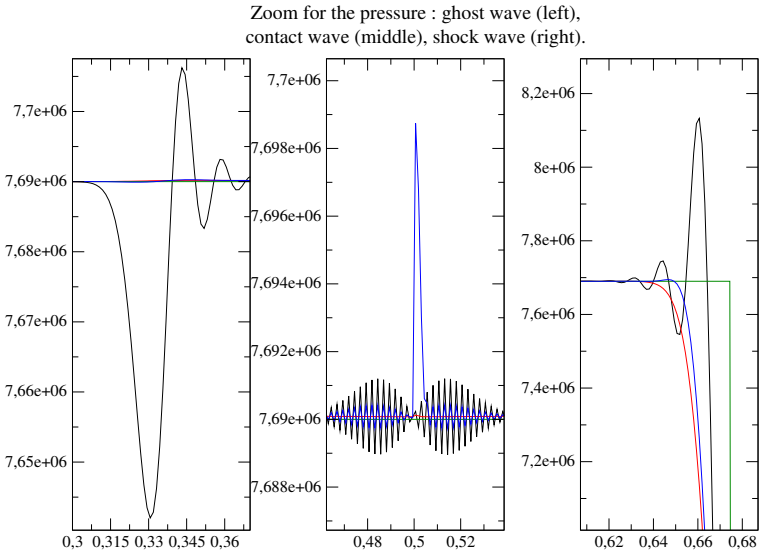

Figure 6: Comparison of the approximate solutions on a mesh with 800 cells, zoom at the wave locations for VFROENCV (red), VFROENCV-C (black), SEMI-IMP at $CFL_{U+C} = 0.5$ (blue). The analytical solution is in green.

4.2 A steady state test case

This test case consists in heating a mixture of water and vapor, assuming that the source terms for the fractions are equal to zero. The heating of the mixture is ensured by an external source term in the energy equation. The computation of the corresponding steady state for system (1) is reported in appendix A. Due to the complex mixture equation of state of the model, the solution at each x is obtained by the mean of a Quasi-Newton algorithm. The boundary conditions are Dirichlet conditions filled with the exact solution. The initial conditions are also the exact solution for all x. The iterations are stopped when the relative L_1-norm between the variables $\Psi \in \{Y, \tau, U, P\}$ at iteration n and $(n-1)$ is less than 10^{-12}:

$$\forall \Psi \in \{Y, \tau, U, P\}, \frac{\sum_{i=1}^{N} |\Psi^{approx}(t^n, x_i) - \Psi^{approx}(t^{n-1}, x_i)|}{\sum_{i=1}^{N} |\Psi^{approx}(t^{n-1}, x_i)|} < 10^{-12}.$$

The domain is $x \in [0, 8\ m]$. The meshes contain from 60 to 12800 cells, except for the SEMI-IMP scheme. Due to the computation time, the finer mesh contains 6400 cells. The source term Φ is applied for $2\ m < x < 6\ m$ and it is uniform within this interval:

$$\Phi(x) = \begin{cases} 5.0\ 10^9\ W/m^3, & \text{if} \quad 2\ m < x < 6\ m, \\ 0, & \text{elsewhere.} \end{cases} \tag{6}$$

At the inlet $x = 0$ the reference state is:

$$\begin{aligned} \rho_0 &= 728.0\ kg/m^3; \\ U_0 &= 5.0\ m/s; \\ P_0 &= 7.69\ 10^6\ Pa; \\ \alpha_0 &= 1.38006860749359\ 10^{-1}; \\ y_0 &= 7.84348344805274\ 10^{-3}; \\ z_0 &= 1.51281566759212\ 10^{-2}; \end{aligned} \tag{7}$$

The analytical solution, which is computed as explained in appendix A, is plotted on figure 7.

Remark 4.1 The reference state corresponds to the left states of the Riemann problem in section 4.1.

From a numerical point of view, the heating source term Φ is integrated using a fractional step approach [19]. The convection terms are first computed and the ODE system including Φ is then integrated by an explicit Euler scheme. For the present steady-state test case with a constant source term, a well-balanced approach could be helpful to improve the accuracy of the VFROENCV scheme. But we are also interested in non constant source terms and unsteady situations for which the fractional step approach remains efficient [10]. We thus focus here on SEMI-IMP and VFROENCV-C schemes which improve the prediction of the steady-state solution as shown on figures (8), (9), (10), (11) and (12).

It should be first mentioned that for all schemes the error between the approximated fractions and the analytical solutions is equal to the round-off errors and is thus not considered in the sequel. The convergence curves are plotted on figure (9). One can note that on coarse meshes VFROENCV-C is less accurate than VFROENCV for the velocity variable, but more accurate for the pressure. As for the problem of section 4.1, the VFROENCV-C scheme still shows an order of convergence of the pressure and velocity greater than the asymptotic order. Due to the discontinuity of the function Φ, a stationary contact wave is introduced in the system of equations, which leads to an asymptotic order of convergence of $1/2$. The latter is recovered on almost all the variables of figure (9), except for the SEMI-IMP scheme for which computations should be pursued on finer meshes.

The results for the different schemes have been plotted on figure (8) for a mesh with 400 cells. The RUSANOV and VFROENCV schemes introduce unphysical pressure gaps at the inlet and outlet of the heating zone (where the source term is discontinuous). These gaps disappear when the mesh is refined (see figure (10)), but on industrial meshes they can lead to unexpected vaporisation/condensation when dealing with mass transfer. The SEMI-IMP ($CFL_{U+C} = 25$) and the VFROENCV-C schemes do not present such important pressure gaps, but oscillations appear arround the location of the sudden change of the heating source term. The amplitude of these oscillations is smaller for the SEMI-IMP scheme, but a more important error is observed in the bulk of the heated zone when compared with the VFROENCV-C scheme. This explains why the error on the pressure variable is greater with the SEMI-IMP scheme compared with the error obtained for the VFROENCV-C (see figure (9)).

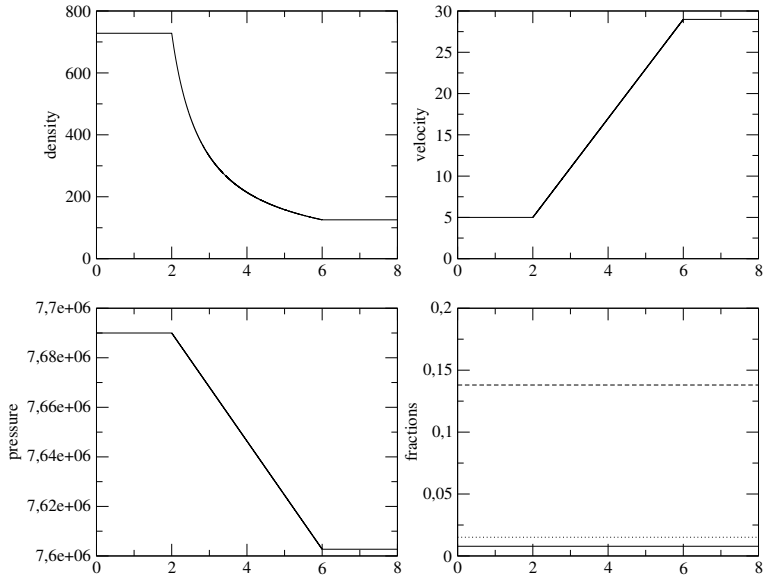

Figure 7: Analytical solution for the steady state heating case.

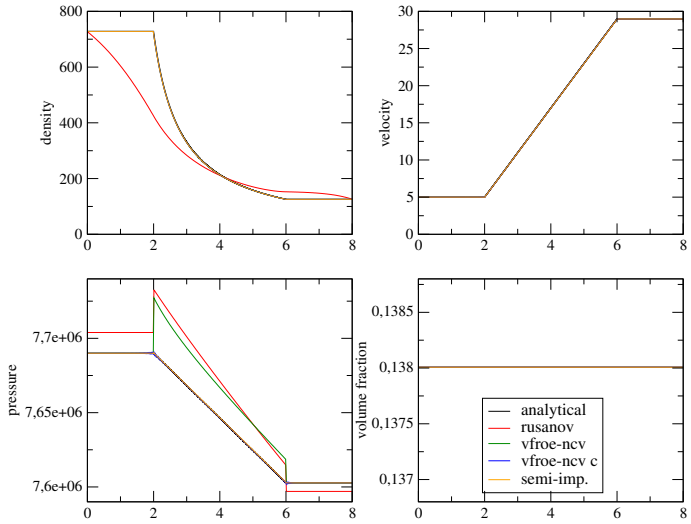

Figure 8: Comparison of the approximated solutions for a mesh with 400 cells. The CFL_{U+C} is equal to 0.5 for the explicit schemes and to 25 for the SEMI-IMP scheme.

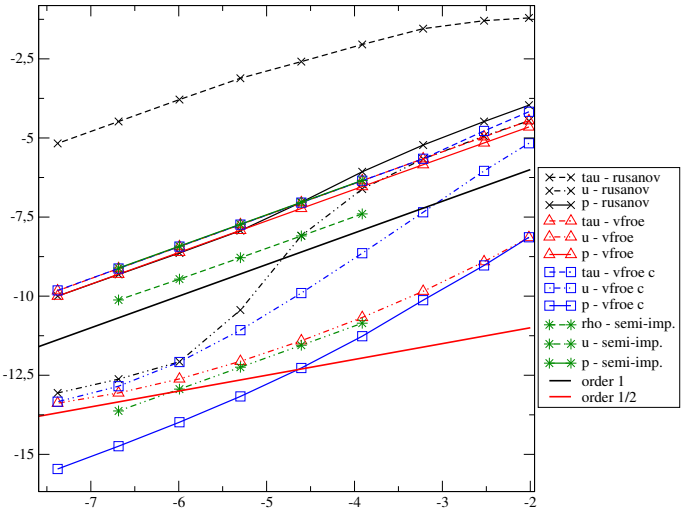

Figure 9: Convergence curves for the steady-state problem: ln() of the L^1 error norm (5) with respect to $\ln(1/N)$ (N number of cells).The CFL_{U+C} is equal to 0.5 for the explicit schemes and to 25 for the SEMI-IMP scheme.

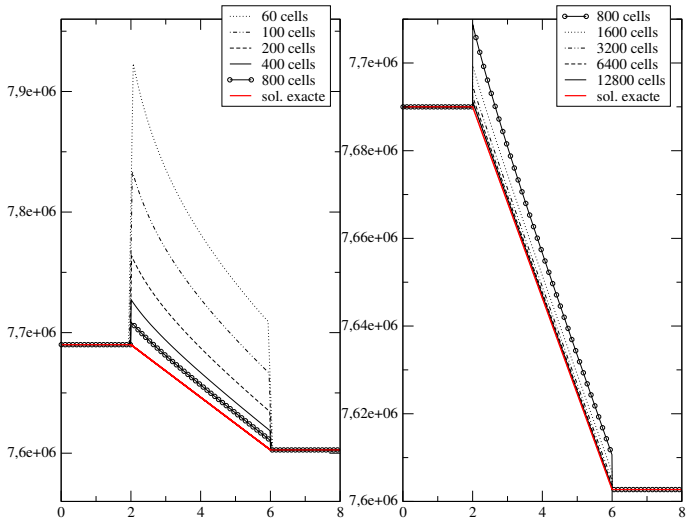

Figure 10: Comparison of the approximated pressure for VFROENCV on different meshes. The CFL_{U+C} is equal to 0.5.

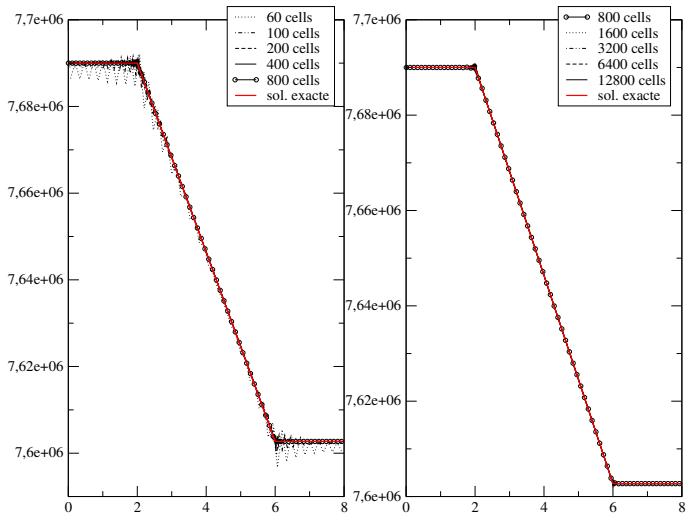

Figure 11: Comparison of the approximated pressure for VFROENCV-C on different meshes. The CFL_{U+C} is equal to 0.5.

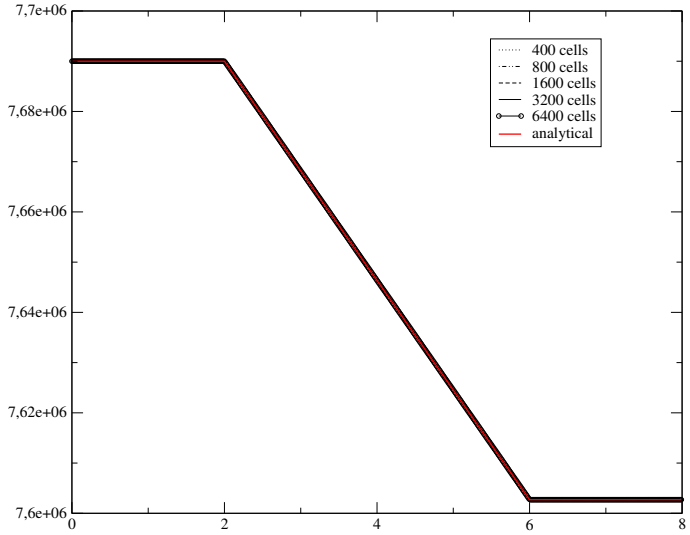

Figure 12: Comparison of the approximated pressure for SEMI-IMP on different meshes and for a time-step corresponding to $CFL_{U+C} = 25$.

5 Conclusion

Four schemes have been tested on two different verification test-cases, which are sketches of industrial configurations. Though the VFROENCV-C scheme presents the best results in terms of the error analysis, the oscillations that appear where discontinuities are computed could be a drawback for industrial purposes. They could for instance be confusing in the case of a configuration where physical oscillations might naturally appear. There are also oscillations in the results obtained with the SEMI-IMP scheme, but their amplitude is smaller on the proposed test cases. On the contrary, the VFROENCV scheme does not generate oscillations, but the main drawback is that it is globally less accurate than the latter two schemes.

Some additional investigations should be performed. In particular a quantitative comparison of the error with respect to the CPU-time would be worthwhile. Actually, if the SEMI-IMP and VFROENCV-C schemes have lower approximation errors for a given mesh size with respect to VFROENCV and RUSANOV, the CPU-time is far greater on the steady-state case of section 4.2. This difference of CPU-time is less important for the unsteady test of section 4.1. Some additional comparisons could also be carried out:

(i) different values of the parameter M_{lim} of the VFROENCV-C scheme ;

(ii) different values of the time-step for the SEMI-IMP scheme ;

(iii) a regular source term Φ ;

(iv) uniform initial conditions and an outlet boundary conditions at $x = 8$.

6 Appendix A: A class of analitycal steady-state solutions for compressible two-phase heated flows

In the following, we extend the solution obtained for single-phase flows in [14] for two-phase flows.

We restrict ourselves to the steady-state solutions of (1) without the source terms S_Y. The variables thus only depend on the space variable x and their space evolution follows the ODE system:

$$\left\{\begin{array}{l} \dfrac{d}{dx}\left(\rho U Y\right) = 0 \\ \dfrac{d}{dx}\left(\rho U\right) = 0 \\ \dfrac{d}{dx}\left(\rho U^2 + P\right) = 0 \\ \dfrac{d}{dx}\left(U(\rho E + P)\right) = \Phi, \end{array}\right. \tag{8}$$

where the thermodynamical behaviour of the mixture is described by a law linking Y, ρ, e and P. We set here $e = \epsilon(Y, \rho, P)$. The source term $\Phi(x)$ denotes an external source of heat and it only depends on the space variable x.

The second equation of (8) states that the mass flow rate ρU is uniform, so that we denote it by $D_0 = \rho U$. The system (8) can thus be written:

$$\left\{\begin{array}{l} D_0 \dfrac{d}{dx}\left(Y\right) = 0 \\ U = \tau D_0 \\ D_0 \dfrac{d}{dx}\left(U\right) + \dfrac{d}{dx}\left(P\right) = 0 \\ D_0 \dfrac{d}{dx}\left(E\right) + \dfrac{d}{dx}\left(UP\right) = \Phi. \end{array}\right. \tag{9}$$

We assume that $D_0 \neq 0$, so that the fractions Y are uniform: $Y = Y_0$. Thanks to the second equation of (9), we replace U by τ in the third and fourth equation of (9). We get the two equations:

$$\left\{\begin{array}{l} D_0^2 \dfrac{d}{dx}\left(\tau\right) + \dfrac{d}{dx}\left(P\right) = 0 \\ D_0 \dfrac{d}{dx}\left(e\right) + \dfrac{D_0^3}{2}\dfrac{d}{dx}\left(\tau^2\right) + D_0 \dfrac{d}{dx}\left(\tau P\right) = \Phi. \end{array}\right. \tag{10}$$

Since the mass flow rate D_0 is uniform and since the source term Φ only depends on x, we can integrate this subsystem as follows on $[x_0, x]$:

$$\begin{cases} D_0^2(\tau - \tau_0) + (P - P_0) = 0 \\ D_0(e - e_0) + \frac{D_0^3}{2}(\tau^2 - \tau_0^2) + D_0(\tau P - \tau_0 P_0) = \int_{x_0}^{x} \Phi(s)ds, \end{cases} \tag{11}$$

where a subscript 0 denotes the value at x_0 which must be given by the user. The symbols without subscript denote the values at a point x. Due to our choice for the equation of states, we have:

$$e = \epsilon(Y, \rho, P) \quad \text{and} \quad e_0 = \epsilon(Y_0, \rho_0, P_0).$$

The first equation of (11) gives explicitly τ as a function of P and since we have $Y = Y_0$, the second equation of (11) is a non linear equation for P:

$$\begin{cases} \tau = \tau_0 - \frac{(P - P_0)}{D_0^2} \\ D_0(\epsilon(Y_0, \frac{1}{\tau}, P) - e_0) - \frac{(P^2 - P_0^2)}{2D_0} = \int_{x_0}^{x} \Phi(s)ds. \end{cases} \tag{12}$$

Hence, solving this equation for P allows to compute the value for τ (with the first equation of (12)), and then, since $D_0 = \rho_0 U_0 = \rho U$, we get U. Obviously, depending on the equation of state ϵ, Φ and D_0, the problem can have one, several or no solution. Moreover it can be complex to solve and it may require the use of numerical algorithm to compute P at each x.

7 Appendix B: The VFROENCV-C and VFROENCV scheme

The VFROENCV and the VFROENCV-C schemes rely on the VFRoe-ncv scheme using the variable (Y, τ, U, P) [2]. Let us first recall the latter algorithm.

For the sake of simplicity, we restrict to regular meshes of size Δx such that: $\Delta x = x_{i+\frac{1}{2}} - x_{i-\frac{1}{2}}$, $i \in \mathbb{Z}$. We denote Δt the time step, where $\Delta t = t^{n+1} - t^n$, $n \in \mathbb{N}$. In order to approximate solutions of the exact solution $W \in \mathbb{R}^p$ of the conservative hyperbolic system:

$$\left\{ \begin{array}{l} \dfrac{\partial}{\partial t}(W) + \dfrac{\partial}{\partial x}(F(W)) = 0 \\ W(x,0) = W_0(x) \end{array} \right.$$

with $F(W)$ in $\mathbb{R}^p$. Let W_i^n be the approximate value of $\dfrac{1}{\Delta x}\displaystyle\int_{x_{i-\frac{1}{2}}}^{x_{i+\frac{1}{2}}} W(x,t^n)dx$. Integrating over $[x_{i-\frac{1}{2}}; x_{i+\frac{1}{2}}] \times [t^n; t^{n+1}]$ provides:

$$W_i^{n+1} = W_i^n - \frac{\Delta t}{\Delta x}\left(\phi_{i+\frac{1}{2}}^n - \phi_{i-\frac{1}{2}}^n\right)$$

The numerical flux $\phi_{i+\frac{1}{2}}^n$ through the interface $\{x_{i+\frac{1}{2}}\} \times [t^n; t^{n+1}]$ is defined below. The time step must agree with a CFL condition detailed below. The flux $\phi_{i+\frac{1}{2}}^n$ depends on W_i^n and W_{i+1}^n when restricting to first order schemes. The approximate Godunov flux $\phi(W_L, W_R)$ is obtained by solving exactly the following linear 1D Riemann problem:

$$\left\{ \begin{array}{l} \dfrac{\partial}{\partial t}(Z) + B(\hat{Z})\dfrac{\partial}{\partial x}(Z) = 0 \\ Z(x,0) = \left\{ \begin{array}{ll} Z_L & \text{if } x < 0 \\ Z_R & \text{otherwise} \end{array} \right. \end{array} \right. \tag{13}$$

with the initial condition: $Z_L = Z(W_i)$ and $Z_R = Z(W_{i+1})$. The matrix:

$$B(Z) = (W_{,Z}(Z))^{-1} A(W(Z))\, W_{,Z}(Z)$$

($A(W)$ is the Jacobian matrix of flux $F(W)$). Once the exact solution $Z^*(\frac{x}{t}; Z_L, Z_R)$ of this approximate problem (13) is obtained, the numerical flux is defined as:

$$\phi(W_L, W_R) = F(W(Z^*(0; Z_L, Z_R)))$$

Let us set $\widetilde{l_k}$, $\widetilde{\lambda_k}$ and $\widetilde{r_k}$, $k = 1, ..., p$, left eigenvectors, eigenvalues and right eigenvectors of matrix $B(\hat{Z})$ respectively. The solution $Z^*(\frac{x}{t}; Z_L, Z_R)$ of the linear Riemann problem is defined everywhere (except along $\frac{x}{t} = \widetilde{\lambda_k}$):

$$\begin{aligned} Z^*\left(\frac{x}{t}; Z_L, Z_R\right) &= Z_L + \sum_{\frac{x}{t} > \widetilde{\lambda_k}} ({}^t\widetilde{l_k}.(Z_R - Z_L))\widetilde{r_k} \\ &= Z_R - \sum_{\frac{x}{t} < \widetilde{\lambda_k}} ({}^t\widetilde{l_k}.(Z_R - Z_L))\widetilde{r_k} \end{aligned}$$

or in a slightly different form:

$$Z_R - Z_L = \sum_{k=1,p} ({}^t\widetilde{l_k}.(Z_R - Z_L))\widetilde{r_k} = \sum_{k=1,p} \tilde{\alpha}_k \widetilde{r_k} \tag{14}$$

setting:

$$\tilde{\alpha}_k = {}^t\,\widetilde{l_k}.(Z_R - Z_L)$$

The only remaining unknown is the mean $\hat{Z}$ which must comply with the condition:

$$\hat{Z}(Z_l = Z_0, Z_r = Z_0) = Z_0$$

The standard average which is used is:

$$\hat{Z}(Z_L, Z_R) = (Z_L + Z_R)/2$$

The explicit form of the approximate Godunov scheme will be under conservative form:

$$W_i^{n+1} - W_i^n + \frac{\Delta t}{\Delta x}\left(F(W(Z^*(0; Z_i^n, Z_{i+1}^n))) - F(W(Z^*(0; Z_{i-1}^n, Z_i^n)))\right) = 0$$

Remark 7.1 A different prediction may be obtained using instead:

$$\hat{Z}(Z_L, Z_R) = Z^*(0; Z_L, Z_R)$$

where the approximate value at the interface $Z^*(0; Z_L, Z_R)$ is obtained solving (13) with:

$$\hat{Z}(Z_L, Z_R) = (Z_L + Z_R)/2$$

This corresponds to the WFRoe-ncv scheme [9].

The two shemes VFROENCV and VFROENCV-C proposed in the sequel are based on the variable change $Z = (Y, \tau, U, P)$. Moreover, the velocity value of the average state $\hat{Z}(Z_L, Z_R) = (Z_L + Z_R)/2$ is replaced by the value of the velocity $U^*(0; Z_L, Z_R)$ which is computed through (13) as in the WFroe-ncv scheme.

At last, for the VFROENCV-C, the pressure $P^*(0; Z_L, Z_R)$ obtained by solving (13) is blended with the centred pressure $(P_L + P_R)/2$ as proposed in [4]. The blending function $f_b(M)$ for the pressure is based on the local Mach number

$$M = |U^*(0; Z_L, Z_R)|/max(C_L, C_R),$$

where C_L and C_R are respectively the left and right sound speeds. We have chosen the function:

$$f_b(M) = \begin{cases} \frac{1-cos(\Pi M/M_{lim})}{2}, & \text{if} \quad M \leq M_{lim}, \\ 1, \quad \text{otherwise.} \end{cases}$$

The modified interfacial pressure P_{LR}^* used to compute the numerical fluxes is then:

$$P_{LR}^* = f_b(M)P^*(0; Z_L, Z_R) + (1 - f_b(M))\frac{P_L + P_R}{2};$$

where P_L and P_R are the left and right pressures. The parameter M_{lim} is the limit mach number above which the pressure correction is not activated.

8 Appendix C: The SEMI-IMP scheme

The algorithm detailed below is based on a fractional step method [19] and follows the classical idea of the so-called pressure correction schemes [3, 16, 18]. Each time step from t^n to t^{n+1} is divided into five steps:

(i) a mass balance step allowing to update the density and to predict an approximation of the pressure;

(ii) a momentum balance step allowing to update the velocity;

(iii) an energy balance step allowing to update the total energy;

(iv) a step for the pure convection of the mixture fractions $Y = \{\alpha, y, z\}$;

(v) and source term step that accounts for the return to the thermodynamical equilibrium.

For each one of the above five steps (i) to (v), the time derivatives are discretized using an implicit Euler scheme. Moreover, the scheme used for the source term step (v) is exactly the same than that used with all the other schemes of the paper [13].

The time step is defined as $\Delta t^n = t^{n+1} - t^n$. By abuse of notation, for any variable Ψ, $\Psi^n = \Psi(t^n)$. Moreover $\Psi^{n+1,-}$ stands for the estimation of the variable Ψ during the fractionnal step, and we set $\delta\Psi = \Psi^{n+1,-} - \Psi^n$. All the variables are then updated (from $t^{n+1,-}$ to t^{n+1}) once the source term step (v) is achieved.

In the following, we set $Q = \rho U$, $\mathcal{E} = \rho E$, and we present the convective part (i.e. steps (i) to (iv)) of the scheme denoted by SEMI-IMP in the paper. It should be mentionned that this algorithm is conservative and it allows then to retrieve the correct shock solutions.

8.1 Mass balance step

In this first step, pressure and density are implicit, while the velocity, the mixture fractions Y and the entropy are considered frozen at time t^n. The convective mass flux is computed as well, it will be noted $\underline{Q}^*$ in order to distinguish it from the mass flux computed at the next step. The mass balance equation is integrated in time between t^n and t^{n+1} and in space over Ω:

$$\int_{t^n}^{t^{n+1}} \int_\Omega \left(\frac{\partial \rho}{\partial t} + \nabla \cdot \underline{Q} \right) d\Omega dt = 0.$$

The two terms of the above equation are treated separately. The divergence term is implicit and Green formula is applied:

$$\int_\Omega \rho(\mathbf{x}, t^{n+1}) - \rho(\mathbf{x}, t^n) d\Omega + \Delta t^n \int_\Gamma \underline{Q}^{n+1} \cdot \underline{n} d\Gamma = 0.$$

In fact, the momentum Q^{n+1} is approximated by the momentum $\underline{Q}^*$ obtained through the following simplified momentum balance equation:

$$\partial_t Q + \nabla P(\rho, s) = 0, \tag{15}$$

which yields:

$$\underline{Q}^* = \underline{Q}^n - \Delta t^n \nabla P^{n+1,-}. \tag{16}$$

The finite volume scheme becomes:

$$vol\,(\Omega)\left(\rho^{n+1,-} - \rho^n\right) + \Delta t^n \int_\Gamma \underline{Q}^* \cdot \underline{n} d\Gamma = 0.$$

It is then assumed that, for a constant entropy, we have:

$$\delta P = \left(c^2\right)^n \delta\rho, \tag{17}$$

with $\left(c^2\right)^n = c^2(P^n, \rho^n)$ (see remark 8.1). This linearization is then used to obtain the form:

$$vol\left(\Omega^\phi\right) \frac{1}{(c^2)^n}(P^{n+1,-} - P^n) + \Delta t^n \int_\Gamma \underline{Q}^*.\underline{n} d\Gamma = 0. \tag{18}$$

Since $\underline{Q}^*$ depends on $P^{n+1,-}$ through equation (16), the pressure $P^{n+1,-}$ can be computed from equation (18). This step then allows to obtain $P^{n+1,-}$, from which $\rho^{n+1,-}$ can be deduced using the relation (17). This update of the density is mandatory in order to ensure the mass conservation.

Remark 8.1 Actually, for non constant entropy s, the relation is $dP = c^2 d\rho + \beta ds$ with $\beta = \frac{\partial P(\rho,s)}{\partial s}$. In the mass balance step, it is thus assumed that the entropy remains constant.

8.2 Momentum balance step

In this second step, the velocity is computed implicitely, while the density and the pressure are known from the previous step; the total energy and the mixture fractions remain steady here. The momentum balance equation is integrated in time between t^n and t^{n+1} and in space over Ω:

$$\int_{t^n}^{t^{n+1}} \int_\Omega \left(\frac{\partial \underline{Q}}{\partial t} + \underline{\nabla} \cdot \left(\underline{u} \otimes \underline{Q}\right) + \underline{\nabla} P \right) d\Omega dt = 0.$$

As for the mass balance step, the different terms of the equations are treated separately. By applying Green formula and using an upwind scheme for the convective term, the following time scheme is obtained:

$$\begin{aligned} vol\,(\Omega)\left(\underline{Q}^{n+1,-} - \underline{Q}^n\right) \quad &+ \quad \Delta t^n \int_\Gamma \left(\underline{u}\left(\underline{Q}.\underline{n}\right)\right)^{n+1,-} d\Gamma \\ &+ \quad \Delta t^n \int_\Gamma P^{n+1,-} \underline{n} d\Gamma = 0. \end{aligned}$$

This step allows to obtain $\underline{u}^{n+1,-}$, and thus $\underline{Q}^{n+1,-} = \rho^{n+1,-}\underline{u}^{n+1,-}$.

Remark 8.2 It is possible to rewrite

$$\underline{Q}^{n+1,-} - \underline{Q}^n = \rho^n(\underline{u}^{n+1,-} - \underline{u}^n) + \underline{u}^{n+1,-}(\rho^{n+1,-} - \rho^n)$$

considering that the increment $(\rho^{n+1,-} - \rho^n)$ is known from the previous step.

8.3 Energy balance step

In this third step, the total energy is computed with a semi-implicit scheme, while the velocity, the pressure and the density are known from the previous steps. The mixture fractions Y still remain constant in this step. The energy balance equation (written in terms of the total energy) is integrated in time between t^n and t^{n+1} and in space over Ω:

$$\int_{t^n}^{t^{n+1}} \int_\Omega \left(\frac{\partial \mathcal{E}}{\partial t} + \nabla \cdot (\underline{u}(\mathcal{E}+P)) - \Phi \right) d\Omega dt = 0,$$

where Φ stands for the external energy source term.

Once again, the terms of the equation are treated separately and Green formula is applied. Using an upwind scheme for the convective term, the following time scheme is deduced:

$$\begin{aligned} vol\,(\Omega)\,(\mathcal{E}^{n+1,-} - \mathcal{E}^n) \quad &+ \quad \Delta t^n \int_\Gamma (\underline{Q}^* \cdot \underline{n}) \left(\frac{\mathcal{E}+P}{\rho} \right)^{n+1,-} d\Gamma \\ &- \quad \Delta t^n vol\,(\Omega)\,\Phi^{n+1,-} = 0. \end{aligned} \tag{19}$$

We use the mass flux $\underline{Q}^*$ computed during the mass balance step in order to ensure the consitency with the mass balance equation.

This step allows to obtain the variable $\mathcal{E}^{n+1,-}$.

8.4 Convection of the mixture fractions Y

In this fourth step, the mixture fractions Y are simply convected using an upwind scheme with the mass flux $\underline{Q}^*$ computed during the mass balance step:

$$vol\,(\Omega)\,\rho^{n+1,-}(Y^{n+1,-} - Y^n) \quad + \quad \Delta t^n \int_\Gamma (\underline{Q}^* \cdot \underline{n}) Y^{n+1,-} d\Gamma = 0.$$

We use the mass flux $\underline{Q}^*$ to ensure the consitency with the mass balance equation.

This step allows to obtain the variable $Y^{n+1,-}$.

8.5 Update of the variables at $t = t^{n+1}$

At the end of each time step, the variables are updated from $t^{n+1,-}$ to t^{n+1} as follows:

$$\begin{aligned} \rho^{n+1} &= \rho^{n+1,-} \\ \underline{u}^{n+1} &= \underline{u}^{n+1,-} \\ \mathcal{E}^{n+1} &= \mathcal{E}^{n+1,-} \\ Y^{n+1} &= Y^{n+1,-} \\ P^{n+1} &= P(Y^{n+1}, \rho^{n+1}, \epsilon^{n+1}) \\ \text{where: } \epsilon^{n+1} &= \frac{\mathcal{E}^{n+1}}{\rho^{n+1}} - \frac{1}{2}(\underline{u}^2)^{n+1} \end{aligned}$$

References

[1] T. Barberon, P. Helluy, "Finite volume simulation of cavitating flows", Computers and Fluids, vol. 34, pp. 832–858, 2005.

[2] Buffard T., Gallouët T., Hérard J.-M., "A sequel to a rough Godunov scheme: application to real gases", Computers and Fluids, Vol. 29 pp. 813–847, 2000.

[3] Chorin A. J., "Numerical solutions of the Navier-Stokes equations", Math. Comp., Vol. 22 pp. 341–353, 1969.

[4] Dellacherie S., "Analysis of Godunov type schemes applied to the compressible Euler system at low Mach number", J. of Comp. Physics, Vol. 229 pp. 978–1016, 2010.

[5] Eymard R., Gallouët T., Herbin R., "The finite volume method", Handbook for Numerical Analysis, Ph. Ciarlet J.L. Lions eds, North Holland, 715–1022, 2000.

[6] Ferrand M., Hérard J.-M., Le Coupanec E., Martin X., "Une formulation intégrale pour la modélisation d'écoulements fluides en milieu encombré", EDF R&D technical report, H-I83-2015-05276-FR (in french), 2015.

[7] Martin X., "Modeling fluid flows in obstructed media", PhD Thesis, Aix Marseille Université, 2015, https://tel.archives-ouvertes.fr/tel-01235089

[8] Gallouët T., Hérard J. M., Seguin N., "Some recent finite volume schemes to compute Euler equations using real gas EOS", Int. J. for Num. Methods in Fluids, Vol. 39(12), pp. 1073–1138, 2002.

[9] Gallouët T., Hérard J.-M., "A new approximate Godunov scheme with application to dense gas-solid flows", Conference: 17th AIAA CFD Conference, Toronto, Canada, 2005, http://dx.doi.org/10.2514/6.2005-4860.

[10] Gallouët T., Hérard J. M., Hurisse O., LeRoux A.Y., "Well-balanced schemes versus fractional step method for hyperbolic systems with source terms", Calcolo, Vol. 43(4), pp. 217–251, 2006.

[11] Godlewski E., Raviart P.-A., "Numerical analysis for hyperbolic systems of conservation laws", Springer Verlag, 1996.

[12] Helluy P., Hérard J.-M., Mathis H., Müller S., "A simple parameter-free entropy correction for approximate Riemann solvers", Comptes Rendus Mécanique, Vol. 388 pp. 493–498, 2010.

[13] Hurisse O., "Application of an homogeneous model to simulate the heating of two-phase flows", Int. J. on Finite Volumes, Vol. 11 pp. 1–37, 2014, https://hal.archives-ouvertes.fr/hal-01114808.

[14] Hurisse O., Le Coupanec E., "A new verification test case for the compressible module of Code_Saturne based on a non trivial steady-state solution for the Euler system with energy", EDF R&D technical report, H-I83-2015-04602-EN, 2015.

[15] Jung J., "Schémas numériques adaptés aux accélérateurs multicœurs pour les écoulements bifluides", PhD. Thesis Strasbourg University (France), 2013, http://tel.archives-ouvertes.fr/tel-00876159.

[16] Patankar S.V., Spalding D.B., "A calculation procedure for heat, mass and momentum transfer in three-dimensional parabolic flows", Int. J. of Heat and Mass Transfer, Vol. 15(10) pp. 1787–1806, 1972.

[17] Rusanov V.V., "Calculations of interaction of non-steady shock waves with obstacles", J. Comp. Math. Phys., Vol. 1 pp. 267–279, 1961.

[18] Temam R., "On an approximate solution of Navier-Stokes equations by the method of fractional step", Arch. Ration. Mech. Anal., Vol. 32 pp. 377–385, 1969.

[19] Yanenko N.N., "Méthode à pas fractionnaires. Résolution de problèmes poly-dimensionnels de physique mathématique", Librairie Armand Colin, 1968.